Article

Not peer-reviewed version

Design, Synthesis, and Acetylcholinesterase Inhibitory Activity of Novel Oxytocin Analogs as Potential Therapeutics for Alzheimer's Disease

Chhanda Charan Danta and Adel Nefzi *

Posted Date: 13 November 2025

doi: 10.20944/preprints202511.0940.v1

Keywords: Alzheimer's disease; acetylcholinesterase; oxytocin; oxytocin-thiazole analogues; acetylcholinesterase inhibitors

 doi:10.20944/preprints202511.0940.v1

Article

Design, Synthesis, and Acetylcholinesterase Inhibitory Activity of Novel Oxytocin Analogs as Potential Therapeutics for Alzheimer's Disease

Chhanda Charan Danta [1] and Adel Nefzi [1,2,*]

[1] Herbert Wertheim College of Medicine, Center for Translational Science, Florida International University, Port Saint Lucie, FL 34987, USA

[2] Department of Chemistry and Biochemistry, College of Arts, Sciences & Education, Florida International University, Miami, FL 33199, USA

* Correspondence: anefzi@fiu.edu

Abstract

Oxytocin (OXT) has demonstrated potential therapeutic effects in Alzheimer's disease (AD) through mechanisms such as reducing amyloid-β (Aβ) accumulation and tau deposition, as well as exerting antioxidant and anti-inflammatory properties. A recent study further revealed that OXT can decrease acetylcholinesterase (AChE) activity in liver and kidney tissues, suggesting that its effects on Aβ and tau pathology may be mediated, at least in part, through AChE inhibition. Based on this rationale, a series of OXT derivatives were designed, synthesized, and evaluated using protein-protein interaction analysis, molecular docking, in vitro AChE inhibition assays, enzyme kinetics, and antioxidant assays. Docking and protein-protein interaction studies showed that OXT and its analogues fit well within the 20 Å gorge of the AChE active site, engaging both the catalytic active site (CAS) and the peripheral anionic site (PAS). In vitro AChE inhibition assays revealed promising activity, with OXT (Cmpd.**16**) and analogue 7 (Cmpd.**7**) exhibiting IC_{50} values of 8.5 μM and 3.6 μM, respectively. Kinetic analysis determined inhibition constants (K_i) of 45 μM for Cmpd.**16** and 6 μM for Cmpd.**7**, with both compounds following a mixed-type inhibition mechanism. Furthermore, antioxidant evaluations indicated potential neuroprotective properties. In conclusion, OXT analogues act as dual-binding site AChE inhibitors, as supported by docking, protein-protein interaction, and kinetic analyses, and display greater inhibitory activity than OXT itself. These findings suggest that OXT analogues represent promising candidates for further development as AChE inhibitors for AD therapy.

Keywords: Alzheimer's disease; acetylcholinesterase; oxytocin; oxytocin-thiazole analogues; acetylcholinesterase inhibitors

1. Introduction

Oxytocin (OXT) is a natural human hormone primarily involved in childbirth and lactation [1–3], but it also plays a key role in social bonding and interpersonal interactions, thereby fostering social relationships and trust within human societies[1,4–8]. Beyond its physiological roles, OXT has been identified as a potential neurobehavioral therapeutic agent due to its strong neuroprotective properties, which include anti-apoptotic, antioxidant, and anti-inflammatory effects in experimental models. Moreover, OXT has been shown to enhance memory and cognition [9–13], making its pharmacological profile highly relevant for Alzheimer's disease (AD) therapy.

AD is a progressive neurodegenerative disorder characterized by cognitive decline, memory loss, and dementia, often accompanied by impaired social behavior. Its neuropathological hallmarks include the accumulation of neurofibrillary tangles, hyperphosphorylated tau, and amyloid-β (Aβ) plaques, all of which contribute to severe neuronal and synaptic damage [14–24]. To date, no curative

 doi:10.20944/preprints202511.0940.v1

or highly selective drug exists for AD treatment. The only clinically validated strategy has been acetylcholinesterase (AChE) inhibition, which provides symptomatic relief by elevating acetylcholine (ACh) levels. FDA-approved AChE inhibitors such as donepezil, rivastigmine, and galantamine although effective to some degrees are small molecules and show only partial clinical benefit [22–25].

Recent studies have highlighted the potential of small peptides as AChE inhibitors [26–29]. In particular, octapeptides have demonstrated promising AChE inhibitory activity, blood–brain barrier permeability, and neuroprotective properties [30]. Similarly, OXT is a nonapeptide (CYIQNCPLG) containing a disulfide bond that forms a cyclic ring via thiol–thiol oxidative coupling of two cysteine residues[31–34] . Although OXT has been reported as an AChE inhibitor, available in vitro inhibition data remain limited[35]. Importantly, OXT has also been shown to reduce tau and Aβ deposition in AD in vivo models[36,37] . Consistent with this, several AChE inhibitors (e.g., donepezil and galantamine) not only increase ACh levels but also reduce Aβ accumulation and potentially influence tau phosphorylation [38–42] . Interestingly, a study in female rats revealed that OXT, either alone or in combination with galantamine, reduced both Aβ and tau deposition [37].

Given these findings, OXT and its analogues being peptides are believed to exert direct effects on the suppression of Aβ and tau pathology. Moreover, molecular pathology suggests a reciprocal relationship between AChE expression and Aβ/tau deposition in AD patients [43]. Therefore, the rationale for investigating OXT and its analogues as potential dual-function AChE inhibitors and neuroprotective agents becomes compelling, as previously proposed in our earlier work [44]. In this study, we report the synthesis of OXT and 15 analogues, their evaluation for AChE inhibition and enzyme kinetics, and the establishment of structure–activity relationships (SARs).

2. Results and Discussion

2.1. Design Strategy of Oxytocin Analogues

Considering the therapeutic importance of OXT in AChE inhibition and its potential in AD treatment, 15 novel analogues were designed and synthesized. To overcome the limitations associated with the disulfide bridge[31,45,46], a rational modification strategy was adopted. Specifically, the fragment (-S-CH_2-CH(NH_2)-CO-) of the OXT structure was replaced with a -S-CH_2-thiazole moiety. The rationale was that the thiazole ring could mimic the therapeutic role of the disulfide bond while offering several advantages: enhanced metabolic and physiological stability, prevention of β-elimination and dimerization, and reduced susceptibility to reduction.

In addition to stabilizing the molecule, incorporation of a thiazole ring was expected to increase lipophilicity, thereby improving blood–brain barrier (BBB) permeability. Structural diversity was further introduced by substituting L-proline (L-Pro) by D-proline (D-Pro). Moreover, combinations of two amino acids asparagine (Asn), glutamine (Gln), or ornithine (Orn) were incorporated at positions R_1 and R_2 to explore their impact on activity. The overall design strategy is illustrated in Figure 1, and the structures of the synthesized analogues are summarized in Table 1.

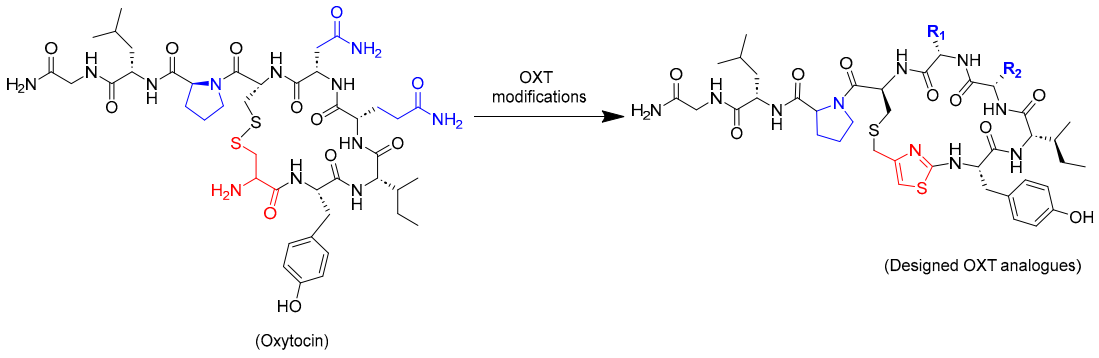

Figure 1. Designing of OXT analogues.

 doi:10.20944/preprints202511.0940.v1

Oxytocin and its analogues were synthesized by solid phase peptide synthesis (SPPS) protocol as described in Scheme 1. Using out "T-bag" technology [47–50], all peptides were synthesized following standard Fmoc peptide synthesis protocol [51–54]. We used the same strategy we reported earlier for the Hantzsch based macrocyclization approach for the synthesis of thiazole containing cyclopeptides [49,55,56].

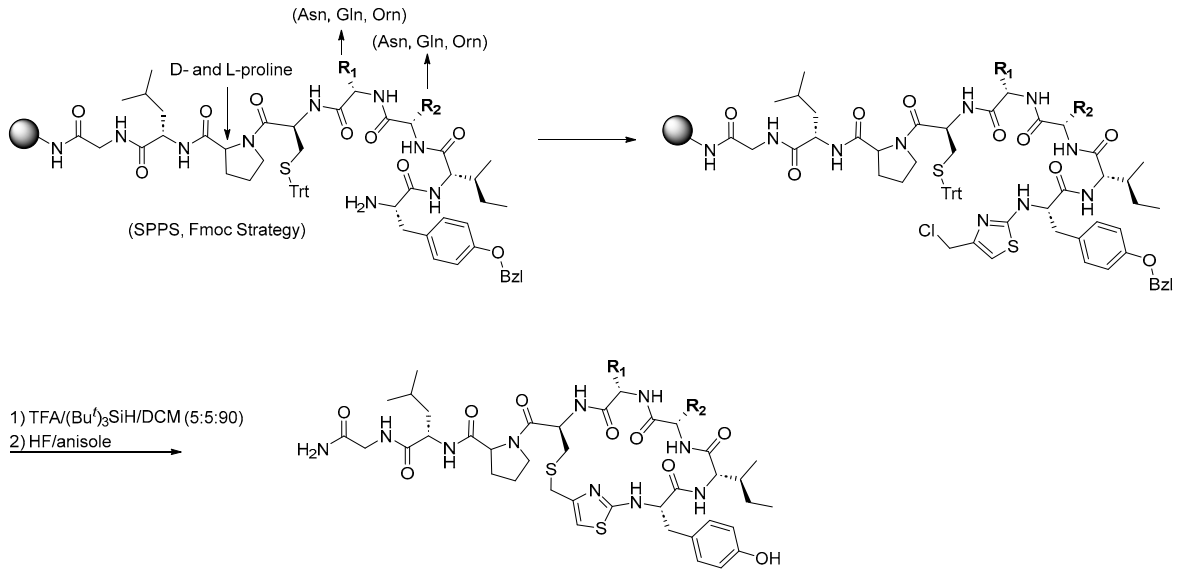

Scheme 1. Synthetic strategy of thiazole containing oxytocin analogues.

Table 1. The synthesized analogues of oxytocin.

Cmpds.	Proline	R_1	R_2
1	L-Pro	Asn	Gln
2	L-Pro	Asn	Asn
3	L-Pro	Asn	Orn
4	L-Pro	Gln	Gln
5	L-Pro	Gln	Asn
6	L-Pro	Gln	Orn
7	L-Pro	Orn	Gln
8	L-Pro	Orn	Asn
9	L-Pro	Orn	Orn
10	D-Pro	Asn	Gln
11	D-Pro	Asn	Asn
12	D-Pro	Asn	Orn
13	D-Pro	Gln	Gln
14	D-Pro	Gln	Asn
15	D-Pro	Gln	Orn
16 (Oxytocin)	Cys-Tyr-Ile-Gln-Asn-Cys-Pro-Leu-Gly-NH_2		

2.2. Protein-Protein Interaction Studies

Protein–protein interaction studies were performed using the ClusPro online docking server to explore the binding interactions between oxytocin (OXT) and human acetylcholinesterase (hAChE,

 doi:10.20944/preprints202511.0940.v1

PDB ID: 7E3H) [57,58] . The three-dimensional structures of OXT (PDB IDs: 1NPO and 7OTD) were individually docked against hAChE in two separate experiments.

In both docking analyses, OXT was found to occupy the active-site gorge of AChE, interacting with residues located in both the catalytic active site (CAS) and the peripheral anionic site (PAS). Two predominant conformers of OXT were identified (Conformer I and Conformer II).

For Conformer I, LigPlot analysis revealed that the tyrosine O–H and C=O groups of OXT formed hydrogen bonds with E202, G121, and Y337 of AChE. The isoleucine C=O and the N–H of glutamine in OXT interacted via hydrogen bonding with Y124 (O–H), while the glutamine N–H atoms also formed hydrogen bonds with the carboxylate group of D74. Notably, both sulfur atoms of OXT participated in hydrogen-bond interactions with the N–H of F295, located in the mid-gorge region of AChE.

In Conformer II, the tyrosine O–H group interacted with W86, while the asparagine residue of OXT formed hydrogen bonds with Y72 and D74, corresponding to interactions at the CAS site. Additionally, both the tyrosine and one cysteine residue of OXT formed hydrogen bonds with W286, representing binding at the PAS region of the active gorge.

Overall, these results suggest that OXT can function as a dual-binding site inhibitor of AChE, engaging both CAS and PAS residues. This dual-site binding profile provides valuable insights for subsequent molecular docking and structure–activity relationship (SAR) studies of the synthesized OXT analogues. The interactions of Conformer I and Conformer II are illustrated in Figure 2a and Figure 2b, respectively (see Supplementary Data).

2.3. Molecular Docking Studies

Following the protein–protein interaction analysis, molecular docking studies were conducted to gain deeper insights into the plausible binding modes and conformations of the synthesized compounds (Cmpds. **1**-**16**) with human acetylcholinesterase (hAChE, PDB ID: 7E3H). Docking simulations were performed using the PyRx Virtual Screening Tool [59].

The co-crystallized complex of hAChE with donepezil (PDB ID: 7E3H) was retrieved from the Protein Data Bank and prepared for docking using AutoDockTools v1.5.7. To validate the docking protocol, the native ligand (donepezil) was redocked into the enzyme's active site. The reproduced pose closely matched the experimental binding conformation, confirming the reliability of the docking setup. Consistent with literature reports, donepezil acted as a dual-binding site inhibitor, occupying both the catalytic active site (CAS) and the peripheral anionic site (PAS) of hAChE.

The chemical structures of the synthesized compounds were drawn using ChemDraw Professional 23.0.1 and saved in. mol format. Prior to docking, both the receptor and all ligand structures were subjected to energy minimization.

Among the series, oxytocin (OXT) exhibited a binding affinity of –7.3 kcal·mol^{-1}, fitting well into the active-site gorge of AChE. OXT formed hydrogen bonds with key residues D74, T83, Q291, S293, and Y337, spanning both the CAS and PAS regions. Additionally, OXT displayed C–H interactions with W86 and E292, π–σ interactions with W286, Y337, and F338, and π–alkyl interactions with H447 (Figure 3). The terminal glycine amide fragment (–$CONH_2$) was involved in three polar hydrogen bonds. Although OXT exhibited a relatively weak π–alkyl non-covalent interaction with H447 (a catalytic triad residue), this interaction, together with surrounding polar hydrogen bonds, could contribute to inhibition of ACh hydrolysis, suggesting a potential neuroprotective mechanism in Alzheimer's disease.

Similarly, OXT analogue **7** showed a slightly higher binding affinity (–7.4 kcal·mol^{-1}) and was well accommodated within the AChE active-site pocket. Analogue 7 formed hydrogen bonds with Y72, T75, and L339 (Figure 4). Its terminal glycine amide group (–$CONH_2$) participated in four polar hydrogen-bond interactions—one more than OXT-likely due to the conformational influence of the incorporated thiazole ring and substitutions at L-Pro, Orn, and Gln residues. These structural modifications may account for its improved binding affinity.

 doi:10.20944/preprints202511.0940.v1

Interestingly, the replacement of the –S–CH_2–CH(NH_2)–CO– fragment in OXT with a thiazole ring in analogue **7** resulted in the loss of two hydrogen bonds but may enhance blood–brain barrier (BBB) permeability and in vivo stability. Both OXT and analogue 7 acted as dual-binding site inhibitors of AChE. The docking results for all synthesized compounds are summarized in **Table 2**.

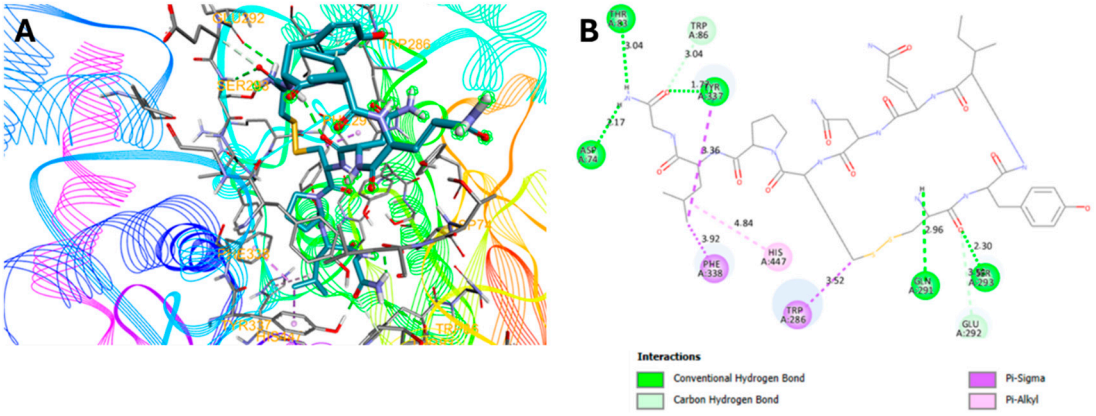

Figure 3. (A) Molecular docking of cmpd. **16** at the active site of hAChE; (B) 2D representation of cmpd.**16** at the active site of hAChE.

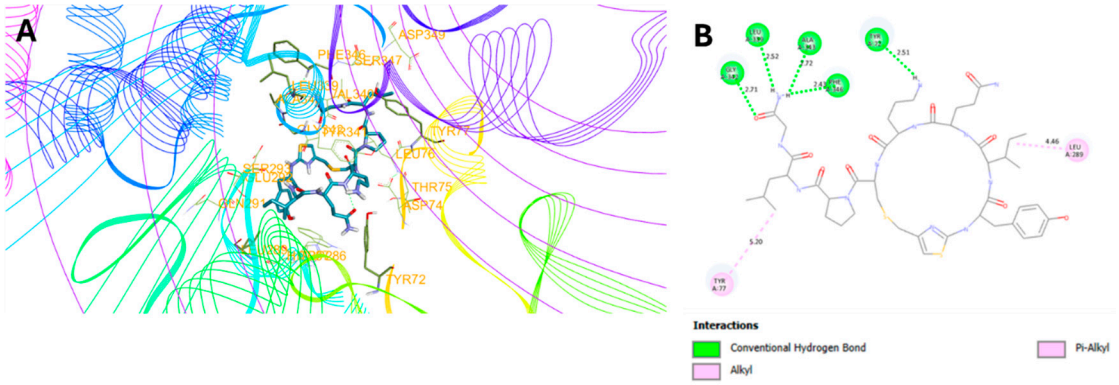

Figure 4. (A) Molecular docking of cmpd.**7** at the active site of hAChE; (B) 2D representation of cmpd.**7** interactions at the active site of hAChE. .

2.4. In Vitro AChE Inhibition Activities

The *in vitro* AChE inhibitory activity of the synthesized compounds (Cmpds. 1-16) was evaluated using a modified Ellman spectrophotometric method [60–63]. For each experiment, the assay mixture (200 µL total volume) consisted of 145 µL of 0.1 M phosphate buffer (pH 8.0), 10 µL of AChE enzyme solution (6 nM in phosphate buffer, pH 8.0), and 5 µL of test compound (dissolved in DMSO at various concentrations). The mixture was incubated at room temperature for 20 min. Subsequently, 10 µL of 5 mM acetylthiocholine iodide (ATCI) solution was added, followed by incubation at 35 °C for 10 min. Finally, 20 µL of 3.3 mM 5,5′-dithiobis(2-nitrobenzoic acid) (DTNB) prepared in 0.1 M phosphate buffer (pH 7.0) containing 6 mM $NaHCO_3$ was added to initiate the reaction. The optical density (O.D.) was measured at 412 nm every 30 s for 3 min using a 96-well microplate reader. Galantamine and rivastigmine were used as reference AChE inhibitors, while 5 µL of neat DMSO served as the negative control. All assays were performed in triplicate. The IC_{50} values were determined by nonlinear regression analysis using GraphPad Prism software. Among the tested compounds, analogue **7** and oxytocin (Cmpd. **16**) exhibited the most potent inhibitory activity, with IC_{50} values of 3.6 µM and 8.5 µM, respectively. Analogue 7 was therefore approximately twofold more potent than OXT. This enhanced activity may be attributed to the presence of a single

 doi:10.20944/preprints202511.0940.v1

aliphatic sulfur atom and a thiazole aromatic ring, which likely improve both binding affinity and complex stability-consistent with the molecular docking observations.

Furthermore, analysis of the IC_{50} data revealed that substitution of D-Pro/L-Pro for proline, and introduction of Asn, Gln, or Orn residues at the R_1 and R_2 positions of the OXT scaffold, generally enhanced AChE inhibitory activity and drug-like characteristics. In contrast, analogue **15**, despite showing favorable binding affinity in docking studies, exhibited a relatively high IC_{50} value, suggesting suboptimal protein–ligand interactions and limited therapeutic potential. The AChE inhibitory IC_{50} values for all synthesized compounds are summarized in Table 2.

Table 2. Docking, AChE inhibition and antioxidant results of the synthesized analogues of oxytocin.

Cmpds.	Binding affinity (Kcal/mol)	No. of H-bonding: (Interacting residues of AChE)	AChE inhibition IC_{50} (μM)*	Antioxidant IC_{50} (μM)*
1	-6.7	4: (V73, W286, G345, F346)	4.6 ± 3.8	54.63 ± 1.2
2	-6.8	6: (V340, W286, G342, F346, Y341, S293)	4.9 ± 4.2	73.19 ± 2.3
3	-5.9	4: (V73, W286, Q279, H287)	4.9 ± 4.1	48.92 ± 1.6
4	-5.3	1: (Q279)	4.9 ± 5.6	76.93 ± 1.6
5	-6.3	3: (T75, L76, S293)	5.4 ± 4.0	76.30 ± 2.4
6	-7.8	8: (V282, V288, W286, H287, L289, G342, A343, F346)	4.4 ± 3.9	46.74 ± 9.1
7	-7.4	5: (Y72, L339, G342, A343, F346)	3.6 ± 4.5	100.5 ± 8.5
8	-6.0	2: (T75, L76)	10.83 ± 6.7	No inhibition
9	-6.5	4: (D74, S293, V340, G342)	60.46 ± 5.1	47.24 ± 5.4
10	-6.9	5: (P88, N87, N89, R90, D131)	5.9 ± 3.9	4.8 ± 6.3
11	-7.5	6: (V73, N283, H287, E292, F346)	10.11 ± 4.7	22.1 ± 4.3
12	-7.1	6: (T75, W286, S293, Y341, F346)	19.71 ± 2.6	31.15 ± 3.3
13	-6.4	7:(Y341, E292, G342, A343, F346)	4.74 ± 2.1	25.82 ± 3.1
14	-7.5	3: (L76, G342, F346)	4.34 ± 1.5	27.41 ± 2.4
15	83.9	3: (T75, V282, W286)	25.36 ± 3.7	25.27 ± 6.2
16 (Oxytocin)	-7.3	5: (D74, T83, Q291, S293, Y337)	8.5 ± 4.5	29.00 ± 2.8
Galantamine	-5.0	1: (Q279)	0.32 ± 5.6	…
Rivastigmine	-5.7	2: (R296, H405)	3.4 ± 22.7	…
Trolox	…	…	…	9.38 ± 0.42
Ascorbic acid	…	…	…	15.53 5.47

2.5. AChE Kinetics Studies

Considering the complex interaction between enzyme and inhibitor, acetylcholinesterase (AChE) kinetics studies were performed to elucidate the mechanism of inhibition[64–66]. The assays were carried out using the same experimental protocol described for the AChE inhibition assay, except that four fixed substrate concentrations of acetylthiocholine iodide (ATCI) (0.125, 0.25, 0.5, and 1.0 mM) were used in combination with varying inhibitor concentrations of the hit compound (Cmpd. **7**) and oxytocin (Cmpd. **16**).

Graphical analysis of the dose–response data and the corresponding Lineweaver–Burk plots demonstrated that the relationship between substrate concentration and reaction velocity conformed to Michaelis–Menten kinetics. The dose–response curve and Lineweaver–Burk plot for Cmpd. **7** are presented in Figures 5 and 6, respectively, while those for Cmpd. **16** are shown in Figures 7 and 8.

 doi:10.20944/preprints202511.0940.v1

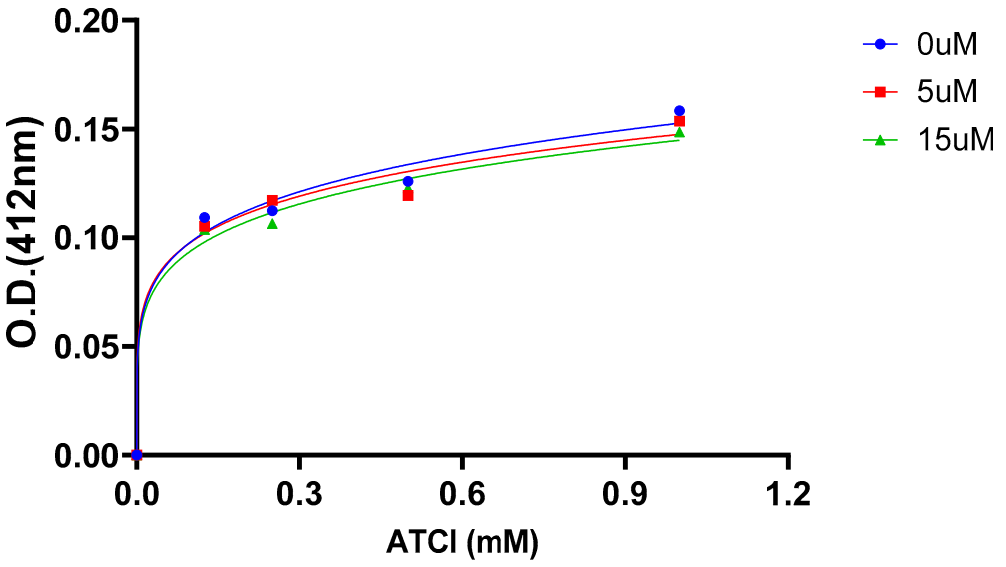

Figure 5. Dose response curve for Cmpd.**7**.

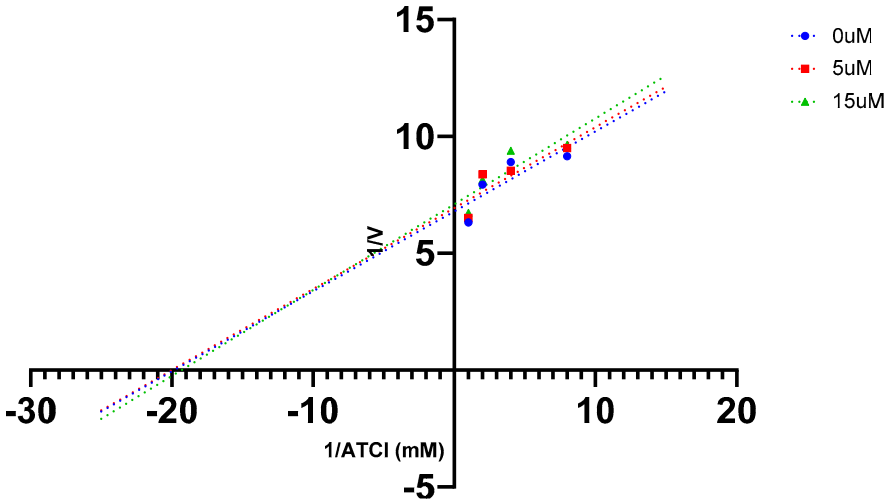

Figure 6. Lineweaver-Burk plot for Cmpd.**7**.

Similarly, the dose–response curve and Lineweaver–Burk plot were generated for Cmpd.**16** (Figure 7 and Figure 8, respectively).

 doi:10.20944/preprints202511.0940.v1

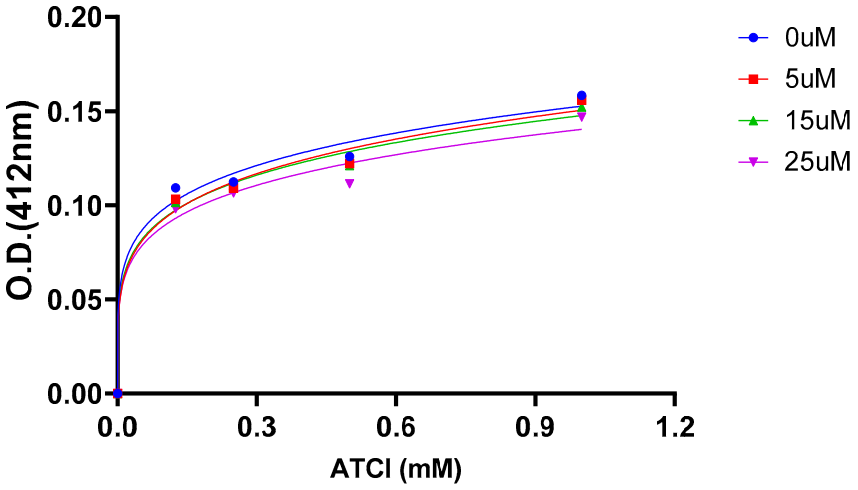

Figure 7. Dose response curve for Cmpd.**16**.

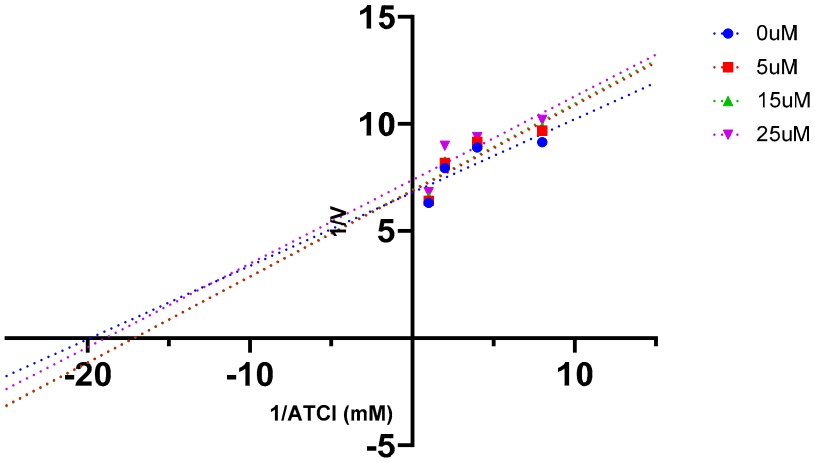

Figure 8. Lineweaver-Burk plot for Cmpd.**16**.

Graphical analysis revealed increasing slopes (indicating decreased Vmax) and increasing intercepts (indicating higher Km) with rising inhibitor concentrations, suggesting a mixed-type inhibition mechanism. Typically, dual-binding-site inhibitors exhibit this pattern, as mixed-type inhibitors can bind both to the free enzyme and to the enzyme–substrate complex at the active site.[67–69]. Therefore, Cmpd.**7** and Cmpd.**16** behaved as dual-binding-site inhibitors. The inhibition constant (Ki) values were determined from the X-intercepts of the plots of Lineweaver–Burk slopes versus inhibitor concentrations. The calculated Ki values for Cmpd.**7** and Cmpd.16 were 6 μM and 45 μM, respectively. These results indicate that Cmpd.**7** exhibits over sevenfold higher binding affinity toward AChE compared to OXT. The corresponding Ki plots are presented in Figure 9 and Figure 10 (Supplementary Data). A summary of the inhibition mechanisms and inhibition constants is provided in Table 3.

Table 3. Inhibition constant and mechanism of inhibition of Cmpd.**7** and Cmpd.**16**.

Cmpds.	Inhibition constant (K_i) (μM)	Mechanism of inhibition
7	6	Mixed type
16 (Oxytocin)	45	Mixed type
Galantamine	5.2	Uncompetitive
Rivastigmine	0.6	Uncompetitive

 doi:10.20944/preprints202511.0940.v1

2.6. Antioxidant Activities

Literature reports indicate that OXT exhibits strong antioxidant potential by activating antioxidant enzyme systems, scavenging free radicals, protecting mitochondrial function, and inhibiting oxidative stress.[9,70] However, its in vitro antioxidant activity has not yet been reported. Therefore, the antioxidant capabilities of OXT analogues were evaluated using a colorimetric method with the free radical reagent; 2,2-diphenyl-1-picrylhydrazyl (DPPH)[71,72]. Ascorbic acid and Trolox were used as reference standards. The corresponding IC_{50} values are listed in Table 2.

The results showed that Cmpd.**16** had an IC_{50} of 29 μM, while Cmpd.**7** had an IC_{50} of 100.5 μM, approximately 3.5-fold lower than OXT. This reduced activity may be attributed to the absence of one sulfur atom, which decreases the availability of free electrons to neutralize DPPH. In contrast, Cmpd.10 exhibited the strongest antioxidant activity among the OXT analogues, with an IC_{50} of 4.8 μM, representing roughly sixfold higher potency than OXT. This enhanced activity may result from the optimal conformation of the substituted D-Pro, Asn, and Gln residues, which positions the aliphatic sulfur atom favorably for DPPH neutralization in the presence of a thiazole ring. These findings suggest that thiazole-containing analogues may have potential as neuroprotective agents similar to OXT.

2.7. In silico physicochemical and ADMET evaluation

In the drug discovery process, predicting the absorption, distribution, metabolism, excretion, and toxicity (ADMET) properties of small molecules during the preclinical stage has become essential, as most drug candidates fail in clinical trials due to suboptimal physicochemical and ADMET characteristics[73]. While Lipinski's Rule of Five provides a useful guideline, it has limitations for peptide-based drugs, which often exhibit higher molecular weights, excessive hydrogen bond donors and acceptors, and a large number of rotatable bonds. Other critical factors-such as blood-brain barrier (BBB) permeability, cellular uptake, gastrointestinal absorption, and metabolic stability-can be evaluated using artificial intelligence (AI)-based in silico tools [74,75]. Some physicochemical and drug-likeness properties of OXT and the active Cmpd.**7** are summarized in **Table 4**. The results indicate that the thiazole substitution in the OXT skeleton improved BBB permeability, cellular uptake, and gastrointestinal absorption. Additionally, Cmpd.**7** exhibited an approximately 1.5-fold higher Log P than OXT, which likely contributes to enhanced BBB penetration.

Table 4. *In silico* ADMET prediction for OXT and Cmpd.**7.**

Compounds		**OXT**	**Cmpd.7**	**Improvement in Cmpd.7 than OXT**
Physicochemical properties	Mol. Wt. (kg/mol)	1006.44	1000.46	…
	Log p o/w (iLog p)	1.72	2.61	1.5-fold higher
Drug-likeness	Caco-2 permeability log(cm/s)	-5.86	-5.72	0.98-fold higher
	Human intestinal absorption (%)	51.93	57.84	1.1-fold higher
	BBB permeability (%)	16.15	16.69	0.54% higher
	Oral bioavailability (%)	37.37	38.85	1.48% higher
	Acute toxicity (LD50) -log(mol/kg)	2.87	3.0	approximate

2.8. SARs

A brief summary of the structure–activity relationships (SARs) of OXT analogues is illustrated in Figure 11. The data indicate that replacing the fragment (-S-CH_2-CH(NH_2)-CO-) with a thiazole

 doi:10.20944/preprints202511.0940.v1

ring enhances both AChE inhibition and binding affinity, while potentially improving CNS penetration. Similarly, substituting proline with L-Pro appears to favor a more optimal molecular conformation, resulting in increased AChE inhibitory activity. Substitutions of Orn at R_1 and Gln at R_2 further improve AChE inhibition. Additionally, the -$CONH_2$ group of the terminal glycine side chain plays a crucial role in hydrogen-bonding interactions within the active-site pocket of AChE. Overall, these modifications collectively enhance the ability of OXT analogues to enter, accommodate, and interact effectively within the active-site gorge of AChE.

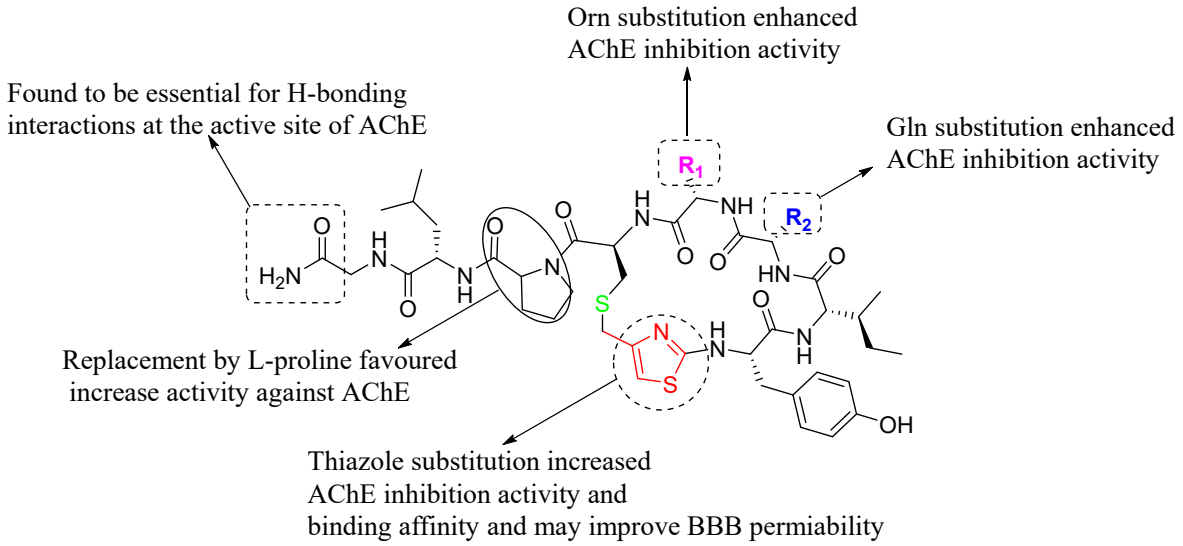

Figure 11. Summary of SARs of OXT analogues as AChE inhibitors.

3. Materials and Methods

3.1. Synthesis of Oxytocin Analogues: As Outlined in Scheme 1, a 100 mg Sample of p-Methylbenzhydrylamine Hydrochloride (MBHA·HCl) Resin (CHEM-IMPEX INTERNATIONAL, 1.15 mequiv/g, 100–200 mesh, 1% DVB) Was Used per Peptide and Enclosed in a Sealed Polypropylene Mesh Bag for the Parallel Synthesis of 16 Different Compounds (Table 1). Prior to Synthesis, the Resin Was Neutralized with 50 mL of 5% Diisopropylethylamine (DIEA) in Dichloromethane (DCM)

All peptides were synthesized via the standard Fmoc solid-phase peptide synthesis (SPPS) method[51,54], involving stepwise Fmoc deprotection and repetitive coupling cycles using *N*-hydroxybenzotriazole (HOBt) and *N,N'*-diisopropylcarbodiimide (DIC) in anhydrous dimethylformamide (DMF). For each coupling reaction, 5 equivalents of Fmoc-protected amino acid, 5 equivalents of DIC, and 5 equivalents of HOBt were used, with the reaction proceeding for 90 min. Fmoc deprotection was performed twice using 20% piperidine in DMF for 10 min each. For cysteine coupling, *L*-Fmoc-Cys(Trt)-OH (5 equivalents) was employed under identical coupling conditions (HOBt/DIC in anhydrous DMF, 90 min). The completion of each coupling step was monitored by the ninhydrin test [76].

For the synthesis of oxytocin (Compound 16), the N-terminal free amine of tyrosine was coupled with Fmoc-Cys(Trt)-OH (5 equiv) in the presence of DIC (5 equiv) and HOBt (5 equiv) as coupling reagents. After completion of coupling, the Fmoc group was removed by treatment with 20% piperidine in DMF (2 × 10 min). Trityl (Trt) deprotection was then carried out using a mixture of trifluoroacetic acid (TFA), triisopropylsilane (TIPS), and dichloromethane (DCM) in a 5:5:90 ratio for 30 min. On-resin disulfide bond formation was achieved by treating the resin with N-chlorosuccinimide (NCS, 3 equiv) in DMF for 30 min [77]. The final product, oxytocin (Compound 16), was cleaved from the resin using anhydrous hydrogen fluoride (HF) in the presence of anisole as a scavenger. The crude peptide was obtained with purity exceeding 90%.

General procedure for the Synthesis of thiazole containing cyclic peptide:

 doi:10.20944/preprints202511.0940.v1

The N-terminal free amine of the resin-bound linear peptide was reacted with Fmoc-isothiocyanate (6 equiv) in anhydrous DMF overnight at room temperature. After Fmoc deprotection using 20% piperidine in DMF, the resulting resin-bound N-terminal thiourea was treated with 1,3-dichloroacetone (5 equiv) in anhydrous DMF at 70 °C for 3 h, affording the resin-bound chloromethyl thiazolyl peptide via Hantzsch cyclocondensation [49,55,56].

Subsequently, the trityl (Trt) protecting group on the cysteine side chain was removed using TFA/TIPS/DCM (5:5:90, v/v/v) for 30 min. The resin was thoroughly washed with DCM (5×) and DIEA/DCM (5:95, v/v), then treated overnight with a solution of Cs_2CO_3 (10 equiv) in DMF to promote intramolecular SN2 cyclization, yielding the cyclic thiazolyl thioether peptide.

The final compounds were cleaved from the resin using HF/anisole (90 min, 0 °C), followed by extraction with 95% aqueous acetic acid and lyophilization to afford the products as white powders. The identity and purity of all compounds were confirmed by LC–MS analysis, with purities exceeding 90%.

3.2. Computational Studies

The protein-protein interaction study was performed using the ClusPro online docking tool (https://cluspro.bu.edu). Molecular docking of ligands was carried out using PyRx–Virtual Screening Tool with AutoDock Vina. The co-crystal structure of human acetylcholinesterase (PDB ID: 7E3H) was obtained from the Protein Data Bank (https://www.rcsb.org/) and prepared for docking using AutoDockTools 1.5.7. Ligand structures were drawn in ChemDraw 23.0.1. The resulting docked complexes, ligand binding modes, and 2D ligand–protein interactions were analyzed using Discovery Studio Visualizer 2024.

3.3. In Silico Prediction

The iLog P values for OXT and Cmpd.7 were calculated using the SwissADME online tool[78]. All other physicochemical and drug-likeness parameters listed in Table 4 were predicted using the AI Drug Lab online platform[79].

3.4. In Vitro Enzyme Inhibition Assays

The AChE inhibition of all synthesized analogues was evaluated using a modified Ellman's method. This assay employs acetylthiocholine iodide (ATCI) as the substrate and 5,5′-dithiobis-(2-nitrobenzoic acid) (DTNB) as the reagent, which produces a yellow chromophore (5-mercapto-2-nitrobenzoic acid) that is detected calorimetrically during the enzymatic reaction. AChE (Electrophorus electricus, Type VI-S, lyophilized powder) was obtained from Sigma-Aldrich (USA), and the stock solution was prepared in 0.1 M sodium phosphate buffer (pH 8.0). The inhibition assay was performed using five different concentrations of each compound dissolved in DMSO. Absorbance at 412 nm was recorded every 30 seconds for 3 minutes using a SpectraMax iD5 plate reader (Molecular Devices) in a 96-well plate format. Galantamine and rivastigmine were included as standard inhibitors. All experiments were conducted in triplicate. Percentage inhibition was calculated as: [(Control absorbance - Test absorbance)/control absorbance]x100. The IC_{50} values for each compound were determined by non-linear regression (four-parameter, variable slope) using GraphPad Prism 10.

3.5. Enzyme Kinetics Assays

Enzyme kinetics were evaluated using four concentrations of the substrate ATCI (0.125, 0.25, 0.5, and 1.0 mM) in the presence and absence of inhibitors (Cmpds.7 and 16). Lineweaver–Burk double reciprocal plots (1/V vs 1/[ATCI]) were constructed to determine the type of inhibition. The inhibition constant (K_i) was subsequently calculated from the slopes of the Lineweaver–Burk plots plotted against inhibitor concentrations.

 doi:10.20944/preprints202511.0940.v1

3.6. Antioxidant Assays

The antioxidant activities of the synthesized compounds were evaluated using the DPPH (2,2-diphenyl-1-picrylhydrazyl) assay. Trolox (6-hydroxy-2,5,7,8-tetramethylchroman-2-carboxylic acid) and ascorbic acid (Vitamin C) were used as reference standards. Five concentrations of each compound were prepared in DMSO.

For each assay, 200 µL of reaction mixture was prepared, containing 185 µL dry ethanol, 5 µL of the test compound, and 10 µL of DPPH solution (10 mM in dry ethanol). The control contained 5 µL of DMSO in dry ethanol. The mixtures were vigorously shaken and incubated at room temperature for 30 min. Absorbance was measured at 517 nm using a SpectraMax iD5 plate reader (Molecular Devices). Lower absorbance of the reaction mixture indicated higher antioxidant activity. All experiments were performed in triplicate. The antioxidant activity (%) was calculated using the formula: [(Control absorbance - Test absorbance)/control absorbance]x100. The rapid color change of DPPH from deep purple to pale yellow in the presence of trolox or ascorbic acid served as the standard observation.

4. Conclusions

In this study, we successfully synthesized oxytocin (OXT) and its analogues following standard peptide synthesis protocols, achieving good to excellent yields and high purity. As no peptide or protein has yet been reported as a standard AChE inhibitor, the activities of the synthesized analogues were primarily compared with OXT and the most active analogue, Cmpd.**7**.

Among the analogues, Cmpd.**7** exhibited the strongest AChE inhibition (IC_{50} = 3.6 µM), approximately twofold more potent than OXT (IC_{50} = 8.5 µM). This enhanced activity is likely due to the thiazole ring substitution and the presence of a single sulfur atom instead of a disulfide bond, consistent with the observed molecular docking binding affinities. In enzyme kinetics, both Cmpd.**7** (K_i = 6 µM) and OXT (K_i = 45 µM) displayed mixed-type inhibition, with Cmpd.**7** showing more than sevenfold higher binding affinity, corroborated by docking scores.

Protein–protein interaction and molecular docking analyses suggested that both compounds can efficiently occupy the active site gorge and interact with both PAS and CAS sites of AChE, supporting their classification as dual binding site inhibitors. The modifications in Cmpd.7 also suggest potentially improved pharmacokinetic and pharmacodynamic properties, including higher BBB permeability and metabolic stability, as estimated by in silico predictions.

Both Cmpd.**7** and OXT demonstrated strong antioxidant activity, likely due to the presence of an aliphatic sulfur atom, whose free electrons can scavenge DPPH radicals, suggesting potential neuroprotective properties. While OXT has been previously reported for its therapeutic potential in Alzheimer's disease, this study provides its first in vitro AChE inhibition and antioxidant data.

Overall, the convenient synthetic strategy allows for the generation of additional OXT analogues to explore structure–activity relationships and develop therapeutic candidates. Further in vivo studies are needed to fully evaluate the potential of OXT and its analogues in the treatment of Alzheimer's disease.

Supplementary Materials: The following supporting information can be downloaded at the website of this paper posted on Preprints.org. Synthetic strategy of thiazole containing oxytocin analogues, Conformer-I and Conformer-II of oxytocin interacting at the active site gorge of AChE, determination of K_i of oxytocin and compound 7. LCMS of all oxytocin analogues.

Author Contributions: C.C.D. conducted *in vitro* assays, statistical analyses, part of design and written the manuscript. A.N was responsible for the overall project planning and design and contributed to writing and revising the manuscript.

Funding: This project was funded by NIH grant 1R61AG086971-01A1 and The Irma & Kalman Bass Neuroscience Research Award.

Conflicts of Interest: The authors declare no conflict of interest.

 doi:10.20944/preprints202511.0940.v1

References

1. Takahashi, J.; Yamada, D.; Nagano, W.; Saitoh, A. The Role of Oxytocin in Alzheimer's Disease and Its Relationship with Social Interaction. *Cells* **2023**, *12* (20). DOI: 10.3390/cells12202426 From NLM.
2. Gimpl, G.; Fahrenholz, F. The oxytocin receptor system: structure, function, and regulation. *Physiol Rev* **2001**, *81* (2), 629-683. DOI: 10.1152/physrev.2001.81.2.629 From NLM.
3. Ishak, W. W.; Kahloon, M.; Fakhry, H. Oxytocin role in enhancing well-being: a literature review. *J Affect Disord* **2011**, *130* (1-2), 1-9. DOI: 10.1016/j.jad.2010.06.001 From NLM.
4. Kosfeld, M.; Heinrichs, M.; Zak, P. J.; Fischbacher, U.; Fehr, E. Oxytocin increases trust in humans. *Nature* **2005**, *435* (7042), 673-676. DOI: 10.1038/nature03701 From NLM.
5. Neal, S.; Kent, M.; Bardi, M.; Lambert, K. G. Enriched Environment Exposure Enhances Social Interactions and Oxytocin Responsiveness in Male Long-Evans Rats. *Front Behav Neurosci* **2018**, *12*, 198. DOI: 10.3389/fnbeh.2018.00198 From NLM.
6. Faraji, J.; Karimi, M.; Soltanpour, N.; Moharrerie, A.; Rouhzadeh, Z.; Lotfi, H.; Hosseini, S. A.; Jafari, S. Y.; Roudaki, S.; Moeeini, R.; et al. Oxytocin-mediated social enrichment promotes longer telomeres and novelty seeking. *Elife* **2018**, *7*. DOI: 10.7554/eLife.40262 From NLM.
7. Kumsta, R.; Heinrichs, M. Oxytocin, stress and social behavior: neurogenetics of the human oxytocin system. *Curr Opin Neurobiol* **2013**, *23* (1), 11-16. DOI: 10.1016/j.conb.2012.09.004 From NLM.
8. Campbell, A. Oxytocin and human social behavior. *Pers Soc Psychol Rev* **2010**, *14* (3), 281-295. DOI: 10.1177/1088868310363594 From NLM.
9. Kamrani-Sharif, R.; Hayes, A. W.; Gholami, M.; Salehirad, M.; Allahverdikhani, M.; Motaghinejad, M.; Emanuele, E. Oxytocin as neuro-hormone and neuro-regulator exert neuroprotective properties: A mechanistic graphical review. *Neuropeptides* **2023**, *101*, 102352. DOI: 10.1016/j.npep.2023.102352 From NLM.
10. Cochran, D. M.; Fallon, D.; Hill, M.; Frazier, J. A. The role of oxytocin in psychiatric disorders: a review of biological and therapeutic research findings. *Harv Rev Psychiatry* **2013**, *21* (5), 219-247. DOI: 10.1097/HRP.0b013e3182a75b7d From NLM.
11. Ceanga, M.; Spataru, A.; Zagrean, A. M. Oxytocin is neuroprotective against oxygen-glucose deprivation and reoxygenation in immature hippocampal cultures. *Neurosci Lett* **2010**, *477* (1), 15-18. DOI: 10.1016/j.neulet.2010.04.024 From NLM.
12. Karelina, K.; Stuller, K. A.; Jarrett, B.; Zhang, N.; Wells, J.; Norman, G. J.; DeVries, A. C. Oxytocin mediates social neuroprotection after cerebral ischemia. *Stroke* **2011**, *42* (12), 3606-3611. DOI: 10.1161/strokeaha.111.628008 From NLM.
13. Vargas-Martínez, F.; Uvnäs-Moberg, K.; Petersson, M.; Olausson, H. A.; Jiménez-Estrada, I. Neuropeptides as neuroprotective agents: Oxytocin a forefront developmental player in the mammalian brain. *Prog Neurobiol* **2014**, *123*, 37-78. DOI: 10.1016/j.pneurobio.2014.10.001 From NLM.
14. Hampel, H.; Mesulam, M. M.; Cuello, A. C.; Farlow, M. R.; Giacobini, E.; Grossberg, G. T.; Khachaturian, A. S.; Vergallo, A.; Cavedo, E.; Snyder, P. J.; et al. The cholinergic system in the pathophysiology and treatment of Alzheimer's disease. *Brain* **2018**, *141* (7), 1917-1933. DOI: 10.1093/brain/awy132 From NLM.
15. Lane, C. A.; Hardy, J.; Schott, J. M. Alzheimer's disease. *European Journal of Neurology* **2018**, *25* (1), 59-70. DOI: https://doi.org/10.1111/ene.13439.
16. Twarowski, B.; Herbet, M. Inflammatory Processes in Alzheimer's Disease-Pathomechanism, Diagnosis and Treatment: A Review. *Int J Mol Sci* **2023**, *24* (7). DOI: 10.3390/ijms24076518 From NLM.
17. Weller, J.; Budson, A. Current understanding of Alzheimer's disease diagnosis and treatment. *F1000Res* **2018**, *7*. DOI: 10.12688/f1000research.14506.1 From NLM.
18. Soria Lopez, J. A.; González, H. M.; Léger, G. C. Alzheimer's disease. *Handb Clin Neurol* **2019**, *167*, 231-255. DOI: 10.1016/b978-0-12-804766-8.00013-3 From NLM.
19. Castellani, R. J.; Perry, G. Pathogenesis and disease-modifying therapy in Alzheimer's disease: the flat line of progress. *Arch Med Res* **2012**, *43* (8), 694-698. DOI: 10.1016/j.arcmed.2012.09.009 From NLM.
20. Mantzavinos, V.; Alexiou, A. Biomarkers for Alzheimer's Disease Diagnosis. *Curr Alzheimer Res* **2017**, *14* (11), 1149-1154. DOI: 10.2174/1567205014666170203125942 From NLM.

 doi:10.20944/preprints202511.0940.v1

21. Ogbodo, J. O.; Agbo, C. P.; Njoku, U. O.; Ogugofor, M. O.; Egba, S. I.; Ihim, S. A.; Echezona, A. C.; Brendan, K. C.; Upaganlawar, A. B.; Upasani, C. D. Alzheimer's Disease: Pathogenesis and Therapeutic Interventions. *Curr Aging Sci* **2022**, *15* (1), 2-25. DOI: 10.2174/1874609814666210302085232 From NLM.
22. Akıncıoğlu, H.; Gülçin, İ. Potent Acetylcholinesterase Inhibitors: Potential Drugs for Alzheimer's Disease. *Mini Rev Med Chem* **2020**, *20* (8), 703-715. DOI: 10.2174/1389557520666200103100521 From NLM.
23. Varadharajan, A.; Davis, A. D.; Ghosh, A.; Jagtap, T.; Xavier, A.; Menon, A. J.; Roy, D.; Gandhi, S.; Gregor, T. Guidelines for pharmacotherapy in Alzheimer's disease - A primer on FDA-approved drugs. *J Neurosci Rural Pract* **2023**, *14* (4), 566-573. DOI: 10.25259/jnrp_356_2023 From NLM.
24. Geldmacher, D. S. Treatment of Alzheimer Disease. *Continuum (Minneap Minn)* **2024**, *30* (6), 1823-1844. DOI: 10.1212/con.0000000000001503 From NLM.
25. Athar, T.; Al Balushi, K.; Khan, S. A. Recent advances on drug development and emerging therapeutic agents for Alzheimer's disease. *Mol Biol Rep* **2021**, *48* (7), 5629-5645. DOI: 10.1007/s11033-021-06512-9 From NLM.
26. Prasasty, V.; Radifar, M.; Istyastono, E. Natural Peptides in Drug Discovery Targeting Acetylcholinesterase. *Molecules* **2018**, *23* (9). DOI: 10.3390/molecules23092344 From NLM.
27. Zare-Zardini, H.; Tolueinia, B.; Hashemi, A.; Ebrahimi, L.; Fesahat, F. Antioxidant and cholinesterase inhibitory activity of a new peptide from Ziziphus jujuba fruits. *Am J Alzheimers Dis Other Demen* **2013**, *28* (7), 702-709. DOI: 10.1177/1533317513500839 From NLM.
28. Siano, A.; Garibotto, F. F.; Andujar, S. A.; Baldoni, H. A.; Tonarelli, G. G.; Enriz, R. D. Molecular design and synthesis of novel peptides from amphibians skin acting as inhibitors of cholinesterase enzymes. *J Pept Sci* **2017**, *23* (3), 236-244. DOI: 10.1002/psc.2974 From NLM.
29. Asen, N. D.; Okagu, O. D.; Udenigwe, C. C.; Aluko, R. E. In vitro inhibition of acetylcholinesterase activity by yellow field pea (Pisum sativum) protein-derived peptides as revealed by kinetics and molecular docking. *Front Nutr* **2022**, *9*, 1021893. DOI: 10.3389/fnut.2022.1021893 From NLM.
30. Mondal, P.; Gupta, V.; Das, G.; Pradhan, K.; Khan, J.; Gharai, P. K.; Ghosh, S. Peptide-Based Acetylcholinesterase Inhibitor Crosses the Blood-Brain Barrier and Promotes Neuroprotection. *ACS Chem Neurosci* **2018**, *9* (11), 2838-2848. DOI: 10.1021/acschemneuro.8b00253 From NLM.
31. Wiśniewski, K.; Finnman, J.; Flipo, M.; Galyean, R.; Schteingart, C. D. On the mechanism of degradation of oxytocin and its analogues in aqueous solution. *Biopolymers* **2013**, *100* (4), 408-421. DOI: 10.1002/bip.22260 From NLM.
32. Wiśniewski, K. Design of Oxytocin Analogs. *Methods Mol Biol* **2019**, *2001*, 235-271. DOI: 10.1007/978-1-4939-9504-2_11 From NLM.
33. Kremsmayr, T.; Schober, G.; Kaltenböck, M.; Hoare, B. L.; Brierley, S. M.; Muttenthaler, M. Oxytocin Analogues for the Oral Treatment of Abdominal Pain. *Angew Chem Int Ed Engl* **2024**, *63* (52), e202415333. DOI: 10.1002/anie.202415333 From NLM.
34. Alshanski, I.; Shalev, D. E.; Yitzchaik, S.; Hurevich, M. Determining the structure and binding mechanism of oxytocin-Cu(2+) complex using paramagnetic relaxation enhancement NMR analysis. *J Biol Inorg Chem* **2021**, *26* (7), 809-815. DOI: 10.1007/s00775-021-01897-1 From NLM.
35. Kocyigit, U. M.; Taşkıran, A.; Taslimi, P.; Yokuş, A.; Temel, Y.; Gulçin, İ. Inhibitory effects of oxytocin and oxytocin receptor antagonist atosiban on the activities of carbonic anhydrase and acetylcholinesterase enzymes in the liver and kidney tissues of rats. *J Biochem Mol Toxicol* **2017**, *31* (11). DOI: 10.1002/jbt.21972 From NLM.
36. Wu, G.; Ou, Y.; Feng, Z.; Xiong, Z.; Li, K.; Che, M.; Qi, S.; Zhou, M. Oxytocin attenuates hypothalamic injury-induced cognitive dysfunction by inhibiting hippocampal ERK signaling and Aβ deposition. *Transl Psychiatry* **2024**, *14* (1), 208. DOI: 10.1038/s41398-024-02930-y From NLM.
37. El-Ganainy, S. O.; Soliman, O. A.; Ghazy, A. A.; Allam, M.; Elbahnasi, A. I.; Mansour, A. M.; Gowayed, M. A. Intranasal Oxytocin Attenuates Cognitive Impairment, β-Amyloid Burden and Tau Deposition in Female Rats with Alzheimer's Disease: Interplay of ERK1/2/GSK3β/Caspase-3. *Neurochem Res* **2022**, *47* (8), 2345-2356. DOI: 10.1007/s11064-022-03624-x From NLM.
38. Zhou, S.; Huang, G. The biological activities of butyrylcholinesterase inhibitors. *Biomed Pharmacother* **2022**, *146*, 112556. DOI: 10.1016/j.biopha.2021.112556 From NLM.

 doi:10.20944/preprints202511.0940.v1

39. Colović, M. B.; Krstić, D. Z.; Lazarević-Pašti, T. D.; Bondžić, A. M.; Vasić, V. M. Acetylcholinesterase inhibitors: pharmacology and toxicology. *Curr Neuropharmacol* **2013**, *11* (3), 315-335. DOI: 10.2174/1570159x11311030006 From NLM.
40. Choi, H. J.; Park, J. H.; Jeong, Y. J.; Hwang, J. W.; Lee, S.; Lee, H.; Seol, E.; Kim, I. W.; Cha, B. Y.; Seo, J.; et al. Donepezil ameliorates Aβ pathology but not tau pathology in 5xFAD mice. *Mol Brain* **2022**, *15* (1), 63. DOI: 10.1186/s13041-022-00948-1 From NLM.
41. Bhattacharya, S.; Haertel, C.; Maelicke, A.; Montag, D. Galantamine slows down plaque formation and behavioral decline in the 5XFAD mouse model of Alzheimer's disease. *PLoS One* **2014**, *9* (2), e89454. DOI: 10.1371/journal.pone.0089454 From NLM.
42. Wu, Z.; Zhao, L.; Chen, X.; Cheng, X.; Zhang, Y. Galantamine attenuates amyloid-β deposition and astrocyte activation in APP/PS1 transgenic mice. *Exp Gerontol* **2015**, *72*, 244-250. DOI: 10.1016/j.exger.2015.10.015 From NLM.
43. García-Ayllón, M. S.; Small, D. H.; Avila, J.; Sáez-Valero, J. Revisiting the Role of Acetylcholinesterase in Alzheimer's Disease: Cross-Talk with P-tau and β-Amyloid. *Front Mol Neurosci* **2011**, *4*, 22. DOI: 10.3389/fnmol.2011.00022 From NLM.
44. Danta, C. C.; Chaudhari, P.; Nefzi, A. Targeting Acetylcholinesterase with Oxytocin: A New Avenue in Alzheimer's Disease Therapeutics. *ACS Chem Neurosci* **2025**, *16* (13), 2336-2339. DOI: 10.1021/acschemneuro.5c00383 From NLM.
45. Nolan, M. D.; Shine, C.; Scanlan, E. M.; Petracca, R. Thioether analogues of the pituitary neuropeptide oxytocin via thiol-ene macrocyclisation of unprotected peptides. *Org Biomol Chem* **2022**, *20* (42), 8192-8196. DOI: 10.1039/d2ob01688e From NLM.
46. Hagen, N.; Bizimana, T.; Kayumba, P. C.; Khuluza, F.; Heide, L. Stability of Oxytocin Preparations in Malawi and Rwanda: Stabilizing Effect of Chlorobutanol. *Am J Trop Med Hyg* **2020**, *103* (5), 2129-2141. DOI: 10.4269/ajtmh.20-0255 From NLM.
47. Nefzi, A.; Ostresh, J. M.; Yu, Y.; Houghten, R. A. Combinatorial chemistry: libraries from libraries, the art of the diversity-oriented transformation of resin-bound peptides and chiral polyamides to low molecular weight acyclic and heterocyclic compounds. *J Org Chem* **2004**, *69* (11), 3603-3609. DOI: 10.1021/jo040114j From NLM.
48. Houghten, R. A. General method for the rapid solid-phase synthesis of large numbers of peptides: specificity of antigen-antibody interaction at the level of individual amino acids. *Proc Natl Acad Sci U S A* **1985**, *82* (15), 5131-5135. DOI: 10.1073/pnas.82.15.5131 From NLM.
49. Nefzi, A. Hantzsch based macrocyclization approach for the synthesis of thiazole containing cyclopeptides. *Methods Mol Biol* **2013**, *1081*, 1-11. DOI: 10.1007/978-1-62703-652-8_1 From NLM.
50. Tantak, M. P.; Rayala, R.; Chaudhari, P.; Danta, C. C.; Nefzi, A. Synthesis of Diazacyclic and Triazacyclic Small-Molecule Libraries Using Vicinal Chiral Diamines Generated from Modified Short Peptides and Their Application for Drug Discovery. *Pharmaceuticals* **2024**, *17* (12), 1566.
51. Behrendt, R.; White, P.; Offer, J. Advances in Fmoc solid-phase peptide synthesis. *J Pept Sci* **2016**, *22* (1), 4-27. DOI: 10.1002/psc.2836 From NLM.
52. Fields, G. B. Methods for removing the Fmoc group. *Methods Mol Biol* **1994**, *35*, 17-27. DOI: 10.1385/0-89603-273-6:17 From NLM.
53. Jaradat, D. M. M. Thirteen decades of peptide synthesis: key developments in solid phase peptide synthesis and amide bond formation utilized in peptide ligation. *Amino Acids* **2018**, *50* (1), 39-68. DOI: 10.1007/s00726-017-2516-0 From NLM.
54. Hansen, P. R.; Oddo, A. Fmoc Solid-Phase Peptide Synthesis. *Methods Mol Biol* **2015**, *1348*, 33-50. DOI: 10.1007/978-1-4939-2999-3_5 From NLM.
55. Nefzi, A.; Arutyunyan, S.; Fenwick, J. E. Two-Steps Hantzsch Based Macrocyclization Approach for the Synthesis of Thiazole Containing Cyclopeptides. *J Org Chem* **2010**, *75* (22), 7939-7941. From NLM.
56. Harris, H. M.; Eans, S. O.; Ganno, M. L.; Davis, J. C.; Dooley, C. T.; McLaughlin, J. P.; Nefzi, A. Antinociceptive activity of thiazole-containing cyclized DAMGO and Leu-(Met) enkephalin analogs. *Org Biomol Chem* **2019**, *17* (21), 5305-5315. DOI: 10.1039/c9ob00882a From NLM.

57. Berman, H. M.; Westbrook, J.; Feng, Z.; Gilliland, G.; Bhat, T. N.; Weissig, H.; Shindyalov, I. N.; Bourne, P. E. The Protein Data Bank. *Nucleic Acids Res* **2000**, *28* (1), 235-242. DOI: 10.1093/nar/28.1.235 From NLM.
58. Dileep, K. V.; Ihara, K.; Mishima-Tsumagari, C.; Kukimoto-Niino, M.; Yonemochi, M.; Hanada, K.; Shirouzu, M.; Zhang, K. Y. J. Crystal structure of human acetylcholinesterase in complex with tacrine: Implications for drug discovery. *Int J Biol Macromol* **2022**, *210*, 172-181. DOI: 10.1016/j.ijbiomac.2022.05.009 From NLM.
59. Dallakyan, S.; Olson, A. J. Small-molecule library screening by docking with PyRx. *Methods Mol Biol* **2015**, *1263*, 243-250. DOI: 10.1007/978-1-4939-2269-7_19 From NLM.
60. Ellman, G. L.; Courtney, K. D.; Andres, V., Jr.; Feather-Stone, R. M. A new and rapid colorimetric determination of acetylcholinesterase activity. *Biochem Pharmacol* **1961**, *7*, 88-95. DOI: 10.1016/0006-2952(61)90145-9 From NLM.
61. Khunnawutmanotham, N.; Sooknual, P.; Batsomboon, P.; Ploypradith, P.; Chimnoi, N.; Patigo, A.; Saparpakorn, P.; Techasakul, S. Synthesis, Antiacetylcholinesterase Activity, and Molecular Dynamics Simulation of Aporphine-benzylpyridinium Conjugates. *ACS Med Chem Lett* **2024**, *15* (1), 132-142. DOI: 10.1021/acsmedchemlett.3c00467 From NLM.
62. Asen, N. D.; Aluko, R. E. Acetylcholinesterase and butyrylcholinesterase inhibitory activities of antioxidant peptides obtained from enzymatic pea protein hydrolysates and their ultrafiltration peptide fractions. *J Food Biochem* **2022**, *46* (11), e14289. DOI: 10.1111/jfbc.14289 From NLM.
63. Balkis, A.; Khoa, T.; Lee, Y. Z.; Ng, K. Screening Flavonoids for Inhibition of Acetylcholinesterase Identified Baicalein as the Most Potent Inhibitor. *Journal of Agricultural Science* **2015**, *7*, 26-26. DOI: 10.5539/jas.v7n9p26.
64. Butterworth, P. J. The use of Dixon plots to study enzyme inhibition. *Biochim Biophys Acta* **1972**, *289* (2), 251-253. DOI: 10.1016/0005-2744(72)90074-5 From NLM.
65. Li, J.; Li, F.; Wu, G.; Gui, F.; Li, H.; Xu, L.; Hao, X.; Zhao, Y.; Ding, X.; Qin, X. Acetylcholinesterase inhibitory activity of sesquiterpenoids isolated from Laggera pterodonta. *Front Plant Sci* **2023**, *14*, 1074184. DOI: 10.3389/fpls.2023.1074184 From NLM.
66. Abbasi, M. A.; Hassan, M.; Aziz Ur, R.; Siddiqui, S. Z.; Shah, S. A. A.; Raza, H.; Seo, S. Y. Synthesis, enzyme inhibitory kinetics mechanism and computational study of N-(4-methoxyphenethyl)-N-(substituted)-4-methylbenzenesulfonamides as novel therapeutic agents for Alzheimer's disease. *PeerJ* **2018**, *6*, e4962. DOI: 10.7717/peerj.4962 From NLM.
67. Tanarro, C. M.; Gütschow, M. Hyperbolic mixed-type inhibition of acetylcholinesterase by tetracyclic thienopyrimidines. *J Enzyme Inhib Med Chem* **2011**, *26* (3), 350-358. DOI: 10.3109/14756366.2010.504674 From NLM.
68. Schepetkin, I. A.; Nurmaganbetov, Z. S.; Fazylov, S. D.; Nurkenov, O. A.; Khlebnikov, A. I.; Seilkhanov, T. M.; Kishkentaeva, A. S.; Shults, E. E.; Quinn, M. T. Inhibition of Acetylcholinesterase by Novel Lupinine Derivatives. *Molecules* **2023**, *28* (8). DOI: 10.3390/molecules28083357 From NLM.
69. Malomo, S. A.; Aluko, R. E. Kinetics of acetylcholinesterase inhibition by hemp seed protein-derived peptides. *J Food Biochem* **2019**, *43* (7), e12897. DOI: 10.1111/jfbc.12897 From NLM.
70. Sever, I. H.; Ozkul, B.; Erisik Tanriover, D.; Ozkul, O.; Elgormus, C. S.; Gur, S. G.; Sogut, I.; Uyanikgil, Y.; Cetin, E. O.; Erbas, O. Protective effect of oxytocin through its anti-inflammatory and antioxidant role in a model of sepsis-induced acute lung injury: Demonstrated by CT and histological findings. *Exp Lung Res* **2021**, *47* (9), 426-435. DOI: 10.1080/01902148.2021.1992808 From NLM.
71. Kilic-Kurt, Z.; Konyar, D.; Okur, H.; Kaplan, A.; Boga, M. Some heterocycles connected to substituted piperazine by 1,3,4-oxadiazole linker: Design, synthesis, anticholinesterase and antioxidant activity. *Journal of Molecular Structure* **2025**, *1321*, 139854. DOI: https://doi.org/10.1016/j.molstruc.2024.139854.
72. Güngör, S. A.; Şahin, İ.; Güngör, Ö.; Tok, T. T.; Köse, M. Synthesis, Biological Evaluation and Docking Study of Mono- and Di-Sulfonamide Derivatives as Antioxidant Agents and Acetylcholinesterase Inhibitors. *Chem Biodivers* **2022**, *19* (10), e202200325. DOI: 10.1002/cbdv.202200325 From NLM.
73. van de Waterbeemd, H.; Gifford, E. ADMET in silico modelling: towards prediction paradise? *Nat Rev Drug Discov* **2003**, *2* (3), 192-204. DOI: 10.1038/nrd1032 From NLM.
74. Di, L. Strategic approaches to optimizing peptide ADME properties. *Aaps j* **2015**, *17* (1), 134-143. DOI: 10.1208/s12248-014-9687-3 From NLM.

 doi:10.20944/preprints202511.0940.v1

75. Okella, H.; Okello, E.; Mtewa, A. G.; Ikiriza, H.; Kaggwa, B.; Aber, J.; Ndekezi, C.; Nkamwesiga, J.; Ajayi, C. O.; Mugeni, I. M.; et al. ADMET profiling and molecular docking of potential antimicrobial peptides previously isolated from African catfish, Clarias gariepinus. *Front Mol Biosci* **2022**, *9*, 1039286. DOI: 10.3389/fmolb.2022.1039286 From NLM.
76. Hancock, W. S.; Battersby, J. E. A new micro-test for the detection of incomplete coupling reactions in solid-phase peptide synthesis using 2,4,6-trinitrobenzenesulphonic acid. *Anal Biochem* **1976**, *71* (1), 260-264. DOI: 10.1016/0003-2697(76)90034-8 From NLM.
77. Postma, T. M.; Albericio, F. N-Chlorosuccinimide, an Efficient Reagent for On-Resin Disulfide Formation in Solid-Phase Peptide Synthesis. *Organic Letters* **2013**, *15* (3), 616-619. DOI: 10.1021/ol303428d.
78. Daina, A.; Michielin, O.; Zoete, V. SwissADME: a free web tool to evaluate pharmacokinetics, drug-likeness and medicinal chemistry friendliness of small molecules. *Scientific Reports* **2017**, *7* (1), 42717. DOI: 10.1038/srep42717.
79. Tian, H.; Ketkar, R.; Tao, P. ADMETboost: a web server for accurate ADMET prediction. *J Mol Model* **2022**, *28* (12), 408. DOI: 10.1007/s00894-022-05373-8 From NLM.